Supplementary Online Information

Imaging set-up

A Cell-Vizio (Mauna-Kea Technologies, Paris) was used for all the experiments. The physical principle of the apparatus has been described (Le Goualher et al., 2004; Laemmel et al., 2004). Briefly, a bundle of fiber optics is used to convey the excitation light to the tissue and to collect the emitted fluorescence. Each fiber in the bundle has a core diameter of 1.9 μm, and the average intercore distance is 3.3 μm (**SFig 1C**). An X-Y scanner using a 4 kHz resonant mirror and a 12 Hz galvanometer is used to scan the proximal end of the bundle with a 488 nm laser beam. Sampling frequency is selected to oversample the pattern of the fibers, giving several readings for each fiber (Le Goualher et al., 2004). For each position of the laser beam, the excitation light travels in one fiber towards the distal end, and excites the fluorescence in the tissue. The fluorescence light is collected by the bundle, travels back through the scanner, passes a dichroic filter and is measured by a photodetector (**SFig. 1A**). Thus, only the light collected by the same fiber that conveyed the excitation reaches the detector, thereby rejecting diffusion and out-of-focus light.

Optical Microprobes

The Cell-vizio can use various flexible microprobes. In these experiments, we used S-0650 and S-0300 microprobes of 650 and 300μm diameter, respectively (**Table 1**). The S-0300 was specifically developed for deep brain imaging: in addition to its small diameter, the bare fiber bundle can be either beveled or shaped as a cone (**SFig. 1B**) for easier tissue penetration and to favor contact with the tissues. Spatial calibration of the images is given by the size of the fiber bundle. Images provided by the conically shaped probes were calibrated by measuring the distance between the tip of the probe (the center of the image) and the junction between the cone and the cylindrical part of the probe. This distance was 490 μm for the probe shown in **SFig. 1B**.

Image Processing.

The fiber bundle is continuously scanned by the excitation laser and the synchronization of the scanner and the detector allows to reconstitute a digital image. This raw image is processed to suppress the artifacts inherent to the scanning method and to the image transport through a bundle of fibers using the method described in detail in Le Goualher et al., 2004.

The system is calibrated by acquiring reference images of water and of a fluorescent solution. These images provide a map of each individual fiber in the field as well as autofluorescence and transmission values for each individual fiber. During the recording, raw image are generated from a scanning of the laser across the fiber bundle with oversampling, giving several readings of the fluorescence signal per fiber (**SFig. 1D1, 2**). The first step is to use the map to assign each reading in the raw image to individual fibers, and the fluorescence value assigned to each fiber is then computed from all the values assigned to it by a statistical estimate. The value is corrected by calibration data: the corresponding background fluorescence is subtracted and a factor is applied to normalize for the fiber's transmission efficiency. At the end of this process, the resulting value is assigned to the fiber's center position (**SFig. 1D3**). The second step is to assign the value characterizing each fiber to all pixels close to its center. This creates blocks centered on the fiber centers (**SFig. 1D4**). The last step is to smoothen the edges of the blocks, for the comfort of the image visualization (**SFig. 1D5**). The image processing also corrects for image distortions due to speed changes during the sinusoidal movement of the resonant mirror. The effect of this processing explains the change in aspect ratio between distorted (**SFigs. 1D1,2**) and corrected images (**SFigs. 1D3-1D5**).

Assessment of lateral and axial resolutions

The S type ProFlex probes feature a bare fiber bundle at their tip. They are not equipped with lenses and, therefore, do not focus light onto or into the tissue to be imaged. The lateral resolution of a fiber bundle is limited by the inter-core distance, i.e. the distance between the centers of two neighboring fibers. To evaluate

the effective lateral resolution of ProFlex probes, we first imaged the US Air Force target, a standard Bar Resolving Power Test Chart commonly used in optical laboratories since 1951. It consists of groups of opaque and transparent bars of different sizes and separations. When superimposed on a fluorescent material, and observed with the S probes, it directly gives the minimum linear distance between two distinguishable bars, which is the lateral resolution. **SFig. 1E1** shows the organization of the line pairs on the target, and **SFig. 1E2** illustrates the corresponding image acquired with an S type ProFlex placed into contact with the target, via a thin layer of water. The ProFlex image is a mirror of the pattern because the target was imaged from below. **SFig. 1E3** shows a higher magnification view the smallest target lines (circled in **SFig. 1E2**), as resolved by the ProFlex probe. Line thickness and separation of the groups at the bottom of the image are 3.9 and 3.47 μm, respectively. Lines can be distinguished in the 2 bottom groups of targets, which feature a 1.5 and 1 μm fiber interval between lines, respectively. The actual resolution on a flat and linear pattern is therefore about 3.5 μm.

The FFM system was then tested in a situation closer to our *in vivo* experiments by imaging fluorescent beads in water. A S probe with flat tip with optical properties similar to those of the probes used for the *in vivo* experiments was attached horizontally on the stage of an upright microscope. The tip of the probe was immersed in water, and imaged using a 20X 0.5NA water immersion objective (Olympus) and a digital camera. A fluorescent bead (Molecular Probes) was seized at the bottom of the chamber by succion via a glass micropipette, and moved horizontally at various distances from the fiber tip. The polished tip of the optic fiber behaved like a mirror, reflecting the image of the glass pipette, and allowing to determine the zero position (see **SFig. 2A** (a), top image). We first tried 4 μm diameter beads, as this size was close to the lateral resolution measured above. When the bead touched the fiber, fluorescence was detected by few fibers (see **SFig. 2A** (a), bottom image; red dots indicate fiber centers). The shape of the bead was not resolved, which is expected considering that the intecore distance almost equaled the bead size. As the bead was moved away, the fluorescence intensity dropped by about 40 % within 3 microns, then declined almost exponentially with a decay constant of 41 μm. Even at 20 μm distance, the fluorescence was collected by the same few fibers, indicating that the lateral resolution is relatively independant from the distance.

Larger beads (15 μm) were also tested, since they approximate the size of a cell. The shape of the bead was fully resolved and the size measured on the fluorescence image equaled the actual size of the bead. When the bead was moved away from the fiber, fluorescence intensity also declined exponentially with a decay constant of 49 μm. The size of the fluorescence spot remained relatively constant, being increased by about 30% at 50μm distance. Thus, these *in vitro* experiments show that the image provided by FFM is an axial projection of fluorescent objects present in front of the fiber, with the contribution of the object to the final image declining exponentially with the distance, with a space constant of approximately 50 μm. In the brain, this decay is likely steeper, as excitation and fluorescence light are absorbed and scattered by the tissue, thereby reducing the contribution of remote objects to the measured signal.

Motion artifacts

Microscopy of moving organs, notably those located in the proximity of heart and lungs, is certainly an unresolved challenge, which may be alleviated by the use of microprobes, such as those (ProFlex) that were used here. The probes can be taken in gentle contact with the organs and their flexibility allows for a parallel movement with the organ, hence ensuring a satisfactory stillness of the recorded image, while avoiding mechanical damage to the tissue. Still, in our hands, recording from continuously moving organs was not evident. However, such difficulties were not encountered in the CNS and PNS experiments described here, which involved tissues and organs distant from lungs and heart. Furthermore, many of the images that we recorded displayed no correlation with heart beat or ventilation movements, and functional changes (e.g. in terms of Ca^{2+} transients) had a much slower time frame than these physiological movements, ruling out potential motion artifacts. Eventually, the motion artifacts induced by the experimenter manipulating the probe produced distinctive changes in the image (see **Supplementary Movies 4** and **6**), which were quite different from those observed during the neuronal response (**Supplementary Movie 5**).

Researchers doing 2-photon in vivo calcium imaging have observed blood-pressure related tissue motion. This results from the large pressure differential between the interior medium (blood pressure) and atmospheric pressure in the region of the brain which is exposed for the recording. These movements are suppressed when imaging is performed through an agar block or through the thinned skull (Stosiek et al, 2003), which is what

most scientists now do: the thinned bone supports the pressure gradient and prevents movements of the brain. With our method, we are looking at depths that are more than 10 times the diameter of the skull opening. The pressure gradient is spread over that distance (several millimeter) and is negligible at the tip of the optic fiber. Basically, one can consider that the fiber tip is in an incompressible medium where pressure variations cannot produce movement. In practice, we have looked for such motion artifacts and we found no fluorescence fluctuations that could be correlated with heart beat and breathing.

Analysis of peripheral nerve regeneration

Untreated mice were monitored for neural regeneration as a function of time after crush, using both *in vivo* FFM video recordings and confocal microscopy images of the fixed nerve. In both sets of images, we measured the length of axonal outgrowth, defined as the distance (in mm) from the most distal portion of the india ink-labelled, crushed region and the most distal region of the nerve featuring characteristic YFP-positive degeneration "ovoids" (Pan et al., 2003; Shiraishi et al., 1985). For *in vivo* measurements, the recording probe scanned the saphenous nerve, along a graduated silver wire which was gently positioned parallel to the nerve trunk. Reading the graduations on the video recordings gave the length of axonal outgrowth in the center and along the 2 sides of each nerve. The mean of these 3 measurements was used to compare the different mice and the different time points. For *in vitro* measurements, the nerves were fixed 18h in 4% paraformaldehyde in 0.1 M phosphate buffer, mounted with a drop of 0.02% paraphenylenediamine in glycerol-PBS (2:1), and observed with a LSM 510 confocal microscope (Zeiss). The entire nerve was reconstructed with photographs taken with a 20x objective (**SFig. 3**), and the length of axonal outgrowth was measured along the central and the 2 lateral axes on these photographs, using a Quantimet 500 software (Leica). Three mice were used per time point (days 3, 4 and 5 after crush), and each mouse was evaluated by FCFM before the nerves were processed for confocal microscopy. Thus, these experiments compared the axonal outgrowth of the very same nerves. This peripheral nerve imaging shows additionally that tissue remaining between the tip of the S650 probe and the fluorescent axon did not interfere with repeated imaging of the same animal. In the case of vincristine-treated animals, 5 mice were evaluated by FCFM per time point (days 3, 4, 5, 6, 8 and 15 after crush), and compared to 5 other mice that received only saline. Thus, the experiments provided for a longitudinal study of the very same nerves in different vincristine- and NaCl-injected mice. In all cases, values were compared by analysis of variance, as provided by the SPSS program (SPSS Inc., Chicago, USA).

Evaluation of tissue damage after deep-brain recording.

To evaluate the damage induced by the brain penetration, we tested different probes, and monitored both the survival of the mice after the recording, and the histology of slices of their brain, sampled 2 weeks after the imaging experiment. All animals survived the recording made with the different probes that, however, differed in their adaptability to brain investigation. The bevelled S650 probe was easily introduced down to 4.5 mm into the brain. **SFig. 4A** shows a brain slice cut parallel to the descent axis. Two weeks after the recording, the penetration path made by the probe was still detectable (arrowheads). However, no obvious tissue damage was observed at the site were the tip of the probe was located (arrow), in order to record from a group of lentivirus-labelled neurons (asterisk). These cells do not show signs of degeneration. The S650 bevelled probe also allowed for multiple brain penetrations. Two penetration traces (arrow heads) separated by 300 μm are seen in **SFig. 4B**, again taken 2 weeks after surgery. Many labeled neurons still exhibit a normal morphology both between the traces (asterisks) and in their immediate vicinity (red arrows). This becomes more evident in the high power confocal analysis of **SFig. 4C**: This horizontal section shows the probe penetration in the middle, outlined by arrowheads. In the immediate vicinity, many cells with characteristic morphology (arrows) remain viable at two weeks after the experiment. The S300 probe caused the mildest tissue damage: **SFig. 4D** shows an immunostaining for GFAP 2 weeks after surgery and recording in the VTA, which is located 4.5 mm below the surface of the skull. A light gliosis is apparent on the left side, along the penetration path (arrowheads), as compared with the contralateral, control side (asterisks).

Legends to Supplementary movies

Due to size restrictions in the Supplement, only short, compressed movies can be shown in the EMBO Reports online Supplement. Full length, high resolution movies are available from the authors at http://npa.snv.jussieu.fr

Supplementary Movie 1
After introduction of the fiber-optic probe through a skin incision made in the saphenous area, the tip of the probe was gently applied to the subcutaneous tissue surrounding the saphenous nerve, and imaging was carried out across the perineurium. Single nerve fibers with their endings can be easily identified and followed over long distances, thus allowing for direct *in vivo* investigation.

Supplementary Movie 2
The real-time video sequence shows a penetration of the 300 μm probe into the nasal cavity of a CaMKinase-eGFP transgenic mouse, and the visualization of the olfactory epithelium and olfactory nerve. The motion is due to the manipulator moving the probe in and out of the nostril.

Supplementary Movie 3
The video sequence shows the repeated penetration of the 300 μm probe into the ventral tegmental area of a TH-eGFP transgenic mouse. The same dopaminergic neurons can be visualized repeatedly.

Supplementary Movie 4
The conical probe is descended from the brain surface towards the dentate gyrus. As the probe crosses the fluorescence-labelled cortical surface and descends into the brain, the fluorescence increases from the center towards the edge of the image. The probe descent was stopped at 3850 μm, corresponding to the position of the dentate gyrus. Movie displayed in real time.

Supplementary Movie 5
Recording corresponding to **Fig. 3**. Movie is accelerated: actual duration is 100s.

Supplementary Movie 6
To verify that the fluorescence changes were not motion artifacts, the probe was moved further down the brain, while monitoring fluorescence in real time. The recording showed a pattern very distinct from that observed with the immobile probe during the bicuculline response (compare with Supplementary Movie 5), indicating that the increase in fluorescence that was recorded under the latter condition reflected genuine elevations in the concentration of cytosolic calcium. Also, during the descent of the probe, some fluorescent spots did not move in the field of view, which presumably correspond to cell debris sticking to the fiber tip. These spots were excluded from the analysis.

Supplementary Movie 7
Recording corresponding to **Fig. 4**. Movie is presented accelerated; actual duration is 42s. Electrical stimulation is indicated by the white square.

REFERENCES

Laemmel, E., Genet, M., Le Goualher, G., Perchant, A., Le Gargasson, J.F. and Vicaut, E. (2004) Fibered confocal fluorescence microscopy (Cell-viZio) facilitates extended imaging in the field of microcirculation. A comparison with intravital microscopy. *J Vasc Res*, **41**, 400-411.

Le Goualher, G., Perchant, A., Genet, M., Cavé, C., Viellerobe, B., Bérier, F., Abrat, B. and Ayache, N. (2004) Towards optical biopsies with an integrated fibered confocal fluorescence microscope. In *Lecture Notes in Computer Science*. Springer, Berlin, pp. 761-768.

Pan, Y.A., Misgeld, T., Lichtman, J.W. and Sanes, J.R. (2003) Effects of neurotoxic and neuroprotective agents on peripheral nerve regeneration assayed by time-lapse imaging in vivo. *J Neurosci*, **23**, 11479-11488.

Sawamoto, K., Nakao, N., Kobayashi, K., Matsushita, N., Takahashi, H., Kakishita, K., Yamamoto, A., Yoshizaki, T., Terashima, T., Murakami, F., Itakura, T. and Okano, H. (2001) Visualization, direct isolation, and transplantation of midbrain dopaminergic neurons. *Proc Natl Acad Sci U S A*, **98**, 6423-6428.

Shiraishi, S., Le Quesne, P.M. and Gajree, T. (1985) The effect of vincristine on nerve regeneration in the rat. An electrophysiological study. *J Neurol Sci*, **71**, 9-17.

Stosiek, C., Garaschuk, O., Holthoff, K. and Konnerth, A. (2003) In vivo two-photon calcium imaging of neuronal networks. *Proc Natl Acad Sci U S A*, **100**, 7319-7324.

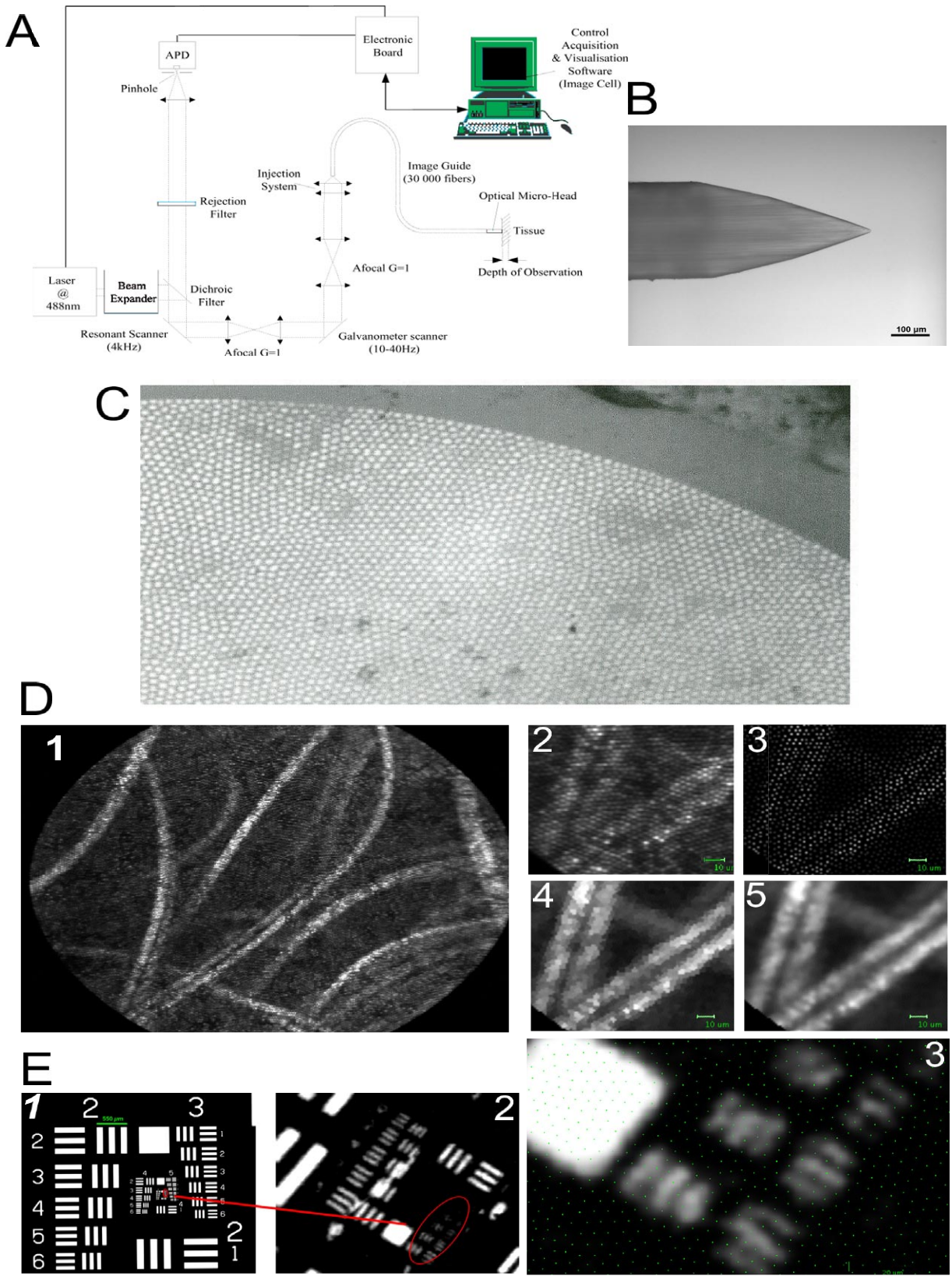

Supplementary Figure 1: Set-up for Fibered Fluorescence Microscopy
(A) Schematic diagram of the Cell-vizio set-up for FFM imaging. (B) Tip of the S-0300 probe which was given a conical shape to favour contact with tissues and easy brain penetration. (C) A microscopic image of the surface of the 650 μm probe, showing the disposition of the 1.9 μm □ fibers. (D) Images of the fiber bundle illustrate the steps of the image processing. D1: raw image of the fiber bundle before image processing. D2: magnified part of D1. D3: the position of each fiber core is assigned the average corrected signal it collected. This signal is expanded (D4) and smoothed to provide the final image (D5). (E) Image of the USAF target used to determine spatial resolution. Green dots in (E3) indicate the center position of each fiber.

Live imaging of neural structure and function by fibered fluorescence microscopy, Vincent et al, EMBO Reports 2006.

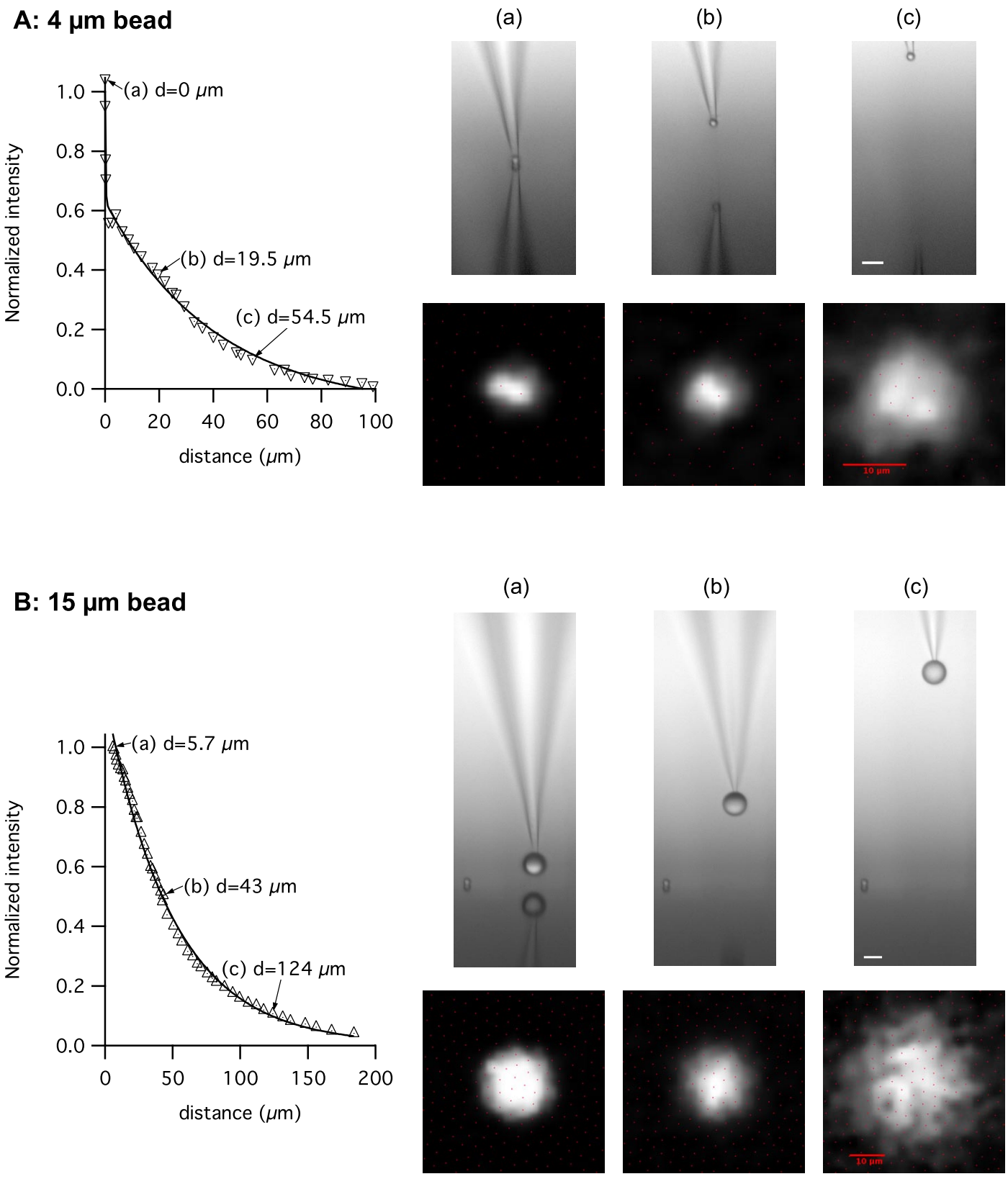

Supplementary Figure 2: Determination of lateral and axial resolution
Fluorescent beads of 4 μm (A) and 15 μm (B) were held by a glass micropipette and moved in front of the tip of the microprobe. The graphs display the normalized intensity as a function of the distance from the edge of the bead to the probe surface. The top images show the pipette and the bead viewed in transmitted light. The mirror image is reflected by the probe tip. The bottom images show the corresponding fluorescence image recorded in parallel by the Cell-Vizio. The red dots indicate the core of the individual fibers within the bundle. The intensity of the signal was quantified by integrating the signal from a circular region of fixed size that encompassed the image of the entire bead at the largest workable distance. Scale bars, 10 μm.

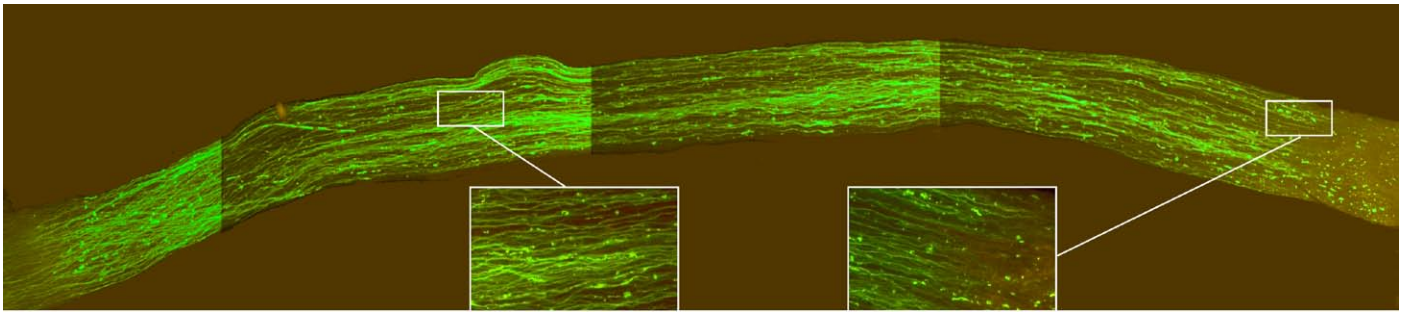

Supplementary Figure 3: Standard confocal microscopy view of a fixed saphenous nerve
The nerve was sampled 4 days after the crush. These images revealed the same morphology of degenerating (right inset) and regenerating fibers (left inset) as shown *in vivo* by FFM (compare left inset with **Fig. 1I** and right inset with **Fig. 1H**). The triangle marks the crush site, exhibiting little fluorescence. The arrow highlights regenerative axons, and the asterisk debris from Wallerian degeneration. Scale bar, 250μm.

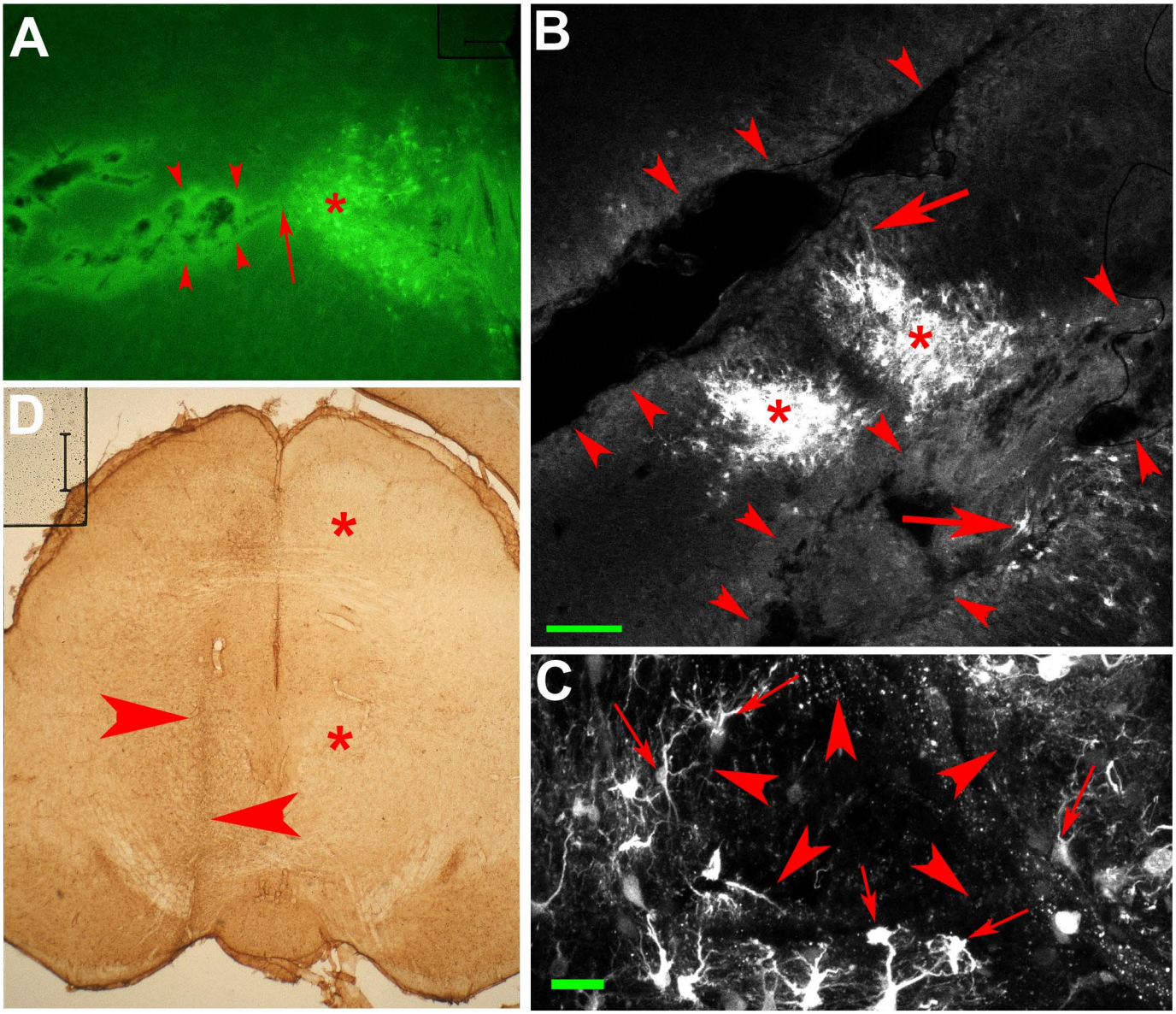

Supplementary Figure 4: Evaluation of tissue damage after deep-brain recording.
(A) Trace of a single penetration of the 650μm probe. Arrowheads mark trace. Arrow indicates tip of the probe. Asterisk marks lentivirus transduced cell group in the VTA. Scalebar, 200μm. (B) Confocal analysis of two closely spaced penetrations of the 650μm probe. Arrowheads mark traces. Asterisks label lentivirus transduced cell group in the dorsal VTA. Arrows point to individual neurons and dendrites. Scalebar, 100μm. (C) High power confocal analysis of cell survival after two weeks. The trace left by the probe is outlined by arrowheads. Many cells in the immediate vicinity exhibit a normal morphology (arrows), showing that they remained viable after the *in vivo* recording. Scalebar, 25μm. (D) Histochemical analysis after deep brain penetration of the 300μm probe. Two weeks after the experiment, GFAP histochemistry was carried out to label reactive astrocytes. Arrowheads, trace of probe. Asterisks, control side showing absence of GFAP label. Scalebar, 400μm.